Advancing Spectrum Sharing through Statistical Analysis of EESS-Passive Satellite Overpasses

Nicholas Brendle
ECE Department
The Ohio State University
Columbus, Ohio
brendle.21@osu.edu

Jonathan Chamberlain
ECE Department
Boston University
Boston, Massachusetts
jdchambo@bu.edu

Joel T. Johnson
ECE Department
The Ohio State University
Columbus, Ohio
johnson.1374@osu.edu

David Starobinski
ECE Department
Boston University
Boston, Massachusetts
staro@bu.edu

Abstract*—Earth-observing measurements performed by Earth Exploration-Satellite Service (EESS) passive satellites are critical to meteorological and climatological assessments of the state of planetary conditions. Radiometers, which perform these measurements, are highly sensitive to anthropogenic transmissions. Therefore, other user access to the spectrum must be carefully managed during an overpass. In this work, we present a statistical characterization of interarrival times and durations of EESS-passive satellite overpasses to support studies between active and passive users co-existing within the radio spectrum. Our work analyzes datasets compiled from multiple EESS-passive satellites to determine the frequency and duration of service interruptions to support the design and evaluation of spectrum sharing approaches. EESS-passive satellite observations that fall within a 100 km region surrounding 15 selected cities are used to produce complementary cumulative density functions (CCDFs) for interarrival times and durations. While the CCDFs for the interruption durations appear location-independent, the interarrival CCDFs demonstrate a high correlation with city latitude due to the nature of EESS-passive orbits. The interarrival time mean and standard deviation are found to be similar and are characterized with simple quadratic functions of latitude that achieve R-squared values of 0.993 and 0.996. The similarity of the mean and standard deviation suggests that a Poisson arrival process (having exponentially distributed interarrival times) is a reasonable assumption in spectrum sharing studies, though more precisely fitted distributions are also discussed. We apply our findings to an economic model of spectrum sharing between EESS-passive and wireless communications services at a given location. We find that the location's latitude has a significant impact on the profitability of the wireless provider.

***Index Terms*—Spectrum access modeling, Datasets for community use, Emerging spectrum co-existence use cases.**

I. Introduction

Earth Exploration-Satellite Service (EESS) passive satellites provide crucial measurements of our planet's land, ocean, and atmosphere that inform weather forecasting models, climate studies, and other applications [1], [2]. It is important that these environmental measurements remain accurate and trustworthy for the sake of accurate short-term forecasts and the maintenance of longer-term climate records. The latter is of particular interest because of the need for monitoring the ongoing evolution of Earth's environmental processes.

EESS-passive radiometers observe background microwave radiation as the signal of interest when recording their measurements. This background radiation is often referred to as "noise" in active systems. The passive nature of radiometer measurements results in a high sensitivity to any presence of active transmissions, making it critical that the sensing environment be free of anthropogenic noise to preserve the accuracy of measurement data. In recent years, modified allocations have been made in and around frequency bands used by radiometers. For example, the 23.8 GHz band is used by radiometers to characterize atmospheric water vapor for meteorological measurements and provide corrections to altimeter measurements. At the World Radiocommunication Conference (WRC) 19, the International Telecommunication Union (ITU) allocated the 24.25-27.5 GHz band for 5G services. At the time of the allocation, 5G was in its early stages of development, making it difficult to assess the effectiveness of the restrictions agreed upon [3], [4]. Allocations such as these can increase unwanted out-of-band emissions in microwave radiometry, resulting in noise-corrupted measurements. In addition to the threat of out-of-band emissions, emissions also occur in bands having only a secondary or no allocation for EESS-passive services. For instance, the 6.425-7.125 GHz band has been widely used by microwave radiometers for measuring sea surface temperatures (SST) due to the sensitivity of SST to changes in emissions in this frequency range. However, at WRC-23 the decision was made to allocate this band for 5G use as well [5], [6].

Conducting a statistical analysis of radiometer arrival frequencies and overpass durations, we find that interarrival times approximately follow an exponential distribution regardless of location, with a strong correlation between latitude and the distribution of interarrival times. Conversely, statistics of overpass durations are insensitive to location and can be described with a common distribution. We note that knowledge of specific corresponding radiometer orbit properties are available, as are information such as radiometer antenna gain and scan patterns. Thus, if a particular radiometer were being modeled, a statistical model would not be necessary because the information on overpass frequency and duration could be derived deterministically from the known information. However, our interest is in the full collection of EESS-passive radiometers operating in a given spatial-frequency domain, not any given radiometer. The relatively large (and increasing) number of observing satellites combined with the utility of statistical descriptions in

TABLE I: EESS radiometers used in the trace data

Satellite	Space Agency	Sensor	Source
Aqua	NASA	AMSU-A	[7]
GCOM-W	JAXA	AMSR2	[8]
GPM Core Observatory	NASA	GMI	[9]
Metop-B	EUMETSAT	AMSU-A	[10]
Metop-C	EUMETSAT	AMSU-A	[10]
NOAA-15	NOAA	AMSU-A	[11]
NOAA-18	NOAA	AMSU-A	[12]
NOAA-19	NOAA	AMSU-A	[12]
JPSS-1 (NOAA 20)	NOAA	ATMS	[13]
JPSS-2 (NOAA 21)	NOAA	ATMS	[13]
SNPP	NOAA	ATMS	[12]
Sentinel-3A	ESA	MWR	[14]
Sentinel-3B	ESA	MWR	[14]
Sentinel-6A	EUMETSTAT	AMR-C	[15]
SWOT	NASA	AMR	[16]

TABLE II: List of cities analyzed and their corresponding number of trace points

City	Latitude	Longitude	Number of Trace Points
Boston, MA	42.36	-71.06	130,108
Columbus, OH	40.00	-83.02	117,187
Dallas, TX	32.78	-96.80	94,615
Mexico City, Mexico	19.42	-99.14	94,615
Quito, Ecuador	-0.25	-78.47	86,786
Pituffik, Greenland	76.53	-68.82	261,252
Fairbanks, AK	64.83	-147.70	230,351
Edmonton, Canada	53.53	-113.50	144,554
Chicago, IL	41.87	-87.64	116,840
Omaha, NE	41.26	-95.95	107,982
Cheyenne, WY	41.14	-104.82	106,340
Salt Lake City, UT	40.76	-111.89	102,997
Barcelona, Spain	41.38	2.17	101,632
Rome, Italy	41.92	12.48	107,936
Sofia, Bulgaria	42.71	23.32	108,676

some applications motivates the statistical treatment reported here. For example, an economic model need not necessarily care about the specific time slots at which frequencies are available, but rather requires information on overall utilization to determine, for example, the level at which to set wholesale spectrum access fees.

We also demonstrate that the EESS-passive service utilization rate is correlated with latitude, with effective utilization in the range 0.4-1% between the Equator and just south of the Arctic Circle (latitude 66.85). These variations in EESS-passive utilization could potentially impact the actions of revenue maximizing providers. Thus, a target location's latitude is an important factor that must be accounted for in economic modeling of EESS-passive spectrum sharing. We provide a concrete example to demonstrate that the correlation between latitude and EESS-passive utilization rates has a significant impact on the corresponding fees and provider profits for commercial users occupying the remaining portions of the spectrum. Remarkably, for certain economic parameters, the difference in profits at different latitudes is many times higher than the difference in utilization rates.

The remainder of this paper is organized as follows. In Section II we review related works discussing our motivating scenario of modeling EESS-passive remote sensing for spectrum co-existence. In Section III we analyze the interarrival times and overpass durations. In Section IV, we discuss Maximum Likelihood Estimation (MLE) fits of the resulting distributions to approximate distributions at arbitrary locations. Finally, in Section V, we apply an example of our findings to an economic model that shows how statistical usage patterns can be leveraged to make utilization assertions without requiring access to specific trace data.

II. Related Work

The competing requirements between active and passive use have expanded as technologies continue to develop and demands for additional bandwidth increase [17]–[19]. While our focus in this work is the remote sensing (EESS-passive) service, such conflicts are also observed in the related passive sensing domain of radio astronomy, where conflicts occur between radio telescopes and commercial satellite clusters operating on the same frequencies [20], [21]. Promoting coexistence that ensures support for EESS-passive applications while maintaining viable access to the predominately commercial active use is essential, and is the subject of multiple prior works in the EESS-passive context [22]–[26]. Several of these references make assumptions about the frequencies and durations of service interruptions, but the arguments advanced by these works can be reinforced by a statistical model for service interruptions.

The work in [27] proposes a joint game-theoretic and queueing-theoretic model for analyzing spectrum sharing scenarios between EESS-passive users and active users. The model is based on the $M/G/1$ queue (i.e., Poisson arrivals and general service distribution). The model is justified through a comparison with a simulation of the queue performance with traces from 14 Earth-observing microwave radiometers in the vicinity of Boston, Massachusetts, USA. A good match in the queueing performance is used to justify the Poisson arrivals assumption for this model. In contrast, in our work, we directly fit statistical distributions to the satellite arrivals and overpass durations data, making the resulting statistical models more broadly applicable and not limited to a specific queueing setting. Another key contribution of our work is in capturing the relationship of these distributions to the latitude of a given location.

III. Statistical Analysis of EESS-Passive Satellites

The data associated with each location in Table II are comprised of all measurements acquired by the 15 microwave radiometers listed in Table I from September 1, 2023 to October 31, 2023 having a reported location within a radius of 100 km from the coordinates in Table II. The reported measurement locations are based on that of the 23.8 GHz channel for each radiometer, but because a 100 km footprint is used around each city, this analysis will remain true for other frequency bands as long as they are available on all radiometers listed in Table I. A plot of these measurement

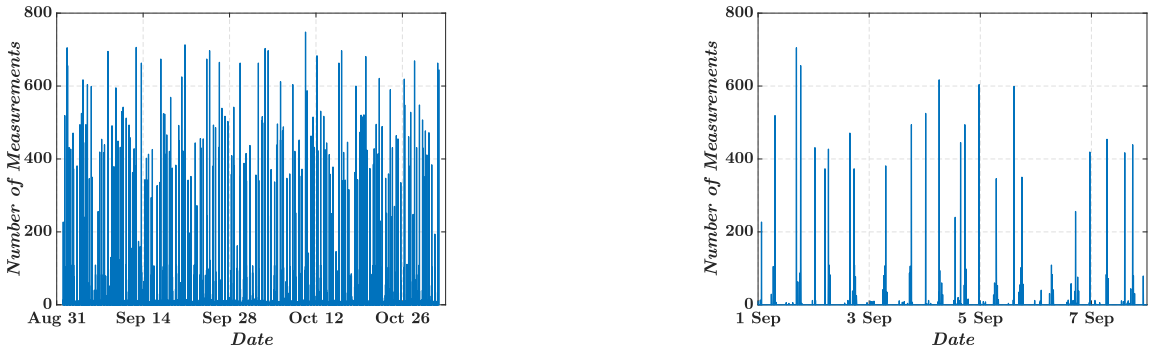

(a) Measurements over two month span

(b) Measurement over selected one week span

Fig. 1: Bar plot of the number of measurements in the 100 km region around Boston, Massachusetts (a) over the two month span of September and October of 2023 and (b) zoomed in on the 1-8 September 2023 time frame. Each bar is a 5 minute interval within that time frame.

data for one of the regions (centered on Boston, MA USA), binned into 5-minute intervals over the two month period, is shown in Fig. 1(a) as an example of the measurement patterns over time. A zoomed-in version is shown in Fig. 1(b). There are two parts of the plot that we want to characterize: the duration of a service interruption and the interarrival times between interruptions.

A. Interarrival Times

In this section, we discuss the statistical characterization of interarrival times, approximately corresponding to the time between each of the bars in Fig. 1. A single interruption typically corresponds to the period of time in which a single low Earth orbiting (LEO) EESS-passive satellite observes the area of interest, which can include multiple measurements reported by the radiometer. The interarrival time then typically corresponds to the interval between satellite overpasses. Reported radiometer measurement times are used in the analysis; the 5 minute binning period in Fig. 1 is used only for simplifying the figure.

For each location, an array of EESS-passive measurement times occurring within 100 km and the satellite conducting the measurement (numbered 1-15) are compiled, with the arrays sorted by time. Using the satellite number array, the time array is divided into 15 separate arrays corresponding to each of the satellites in Table I. Then, each array is put into a logic array spanning the two-month period with half-second bins. Finally, the 15 arrays are put through an or gate, resulting in the final array from which inter-arrival times and durations can be calculated.

Using this method, interarrival times were calculated for each of the 15 cities in Table II. Then a complementary cumulative density function of the interarrival times was generated for each city. Fig. 2(a) illustrates the resulting CCDFs for seven cities spanning latitudes -0.25 and 76.53 degrees. The plot shows that as latitude increases, the distributions become dominated by shorter interarrival times, with the effect becoming particularly pronounced close to and within the Arctic Circle (66.85).

This trend results from the near-polar orbits of most EESS-passive satellites, which result in more frequent overpasses at higher latitudes. By extension, we would expect that locations along the same (or similar) latitude should have similar distributions. In Fig. 2(b) we plot the CCDFs for 9 cities of latitude 40.00 to 42.71 degrees with the corresponding longitudes varying from -111.89 and 23.32 degrees. The high correspondence in the results confirms the similarity of interarrival time properties as a function of longitude.

While the plots in Figs. 2(a) and 2(b) have some features similar to the CCDF of an exponentially distributed random variable, it is apparent that such a distribution would not be a perfect fit, especially when considering more northern latitudes. Further, the behavior of the empirical CCDFs suggests a combination of multiple distributions given the distinct properties of each EESS-passive satellite considered. We discuss this further in Section IV. Rather than attempting more specific distribution fits, we instead perform an analysis of the interarrival time mean and standard deviation.

Fig. 4(a) shows the mean interarrival time μ and standard deviation σ as a function of latitude. The high correlation to latitude is apparent; accordingly a quadratic least squares (LS) regression was developed for each parameter. An R-square value of 0.993 for the mean and 0.996 for the standard deviation fit resulted, with

$$\mu = 1.52 - (2.74 \times 10^{-3})|L| - (1.71 \times 10^{-4})L^2 \quad (1)$$

$$\sigma = 1.80 + (3.08 \times 10^{-3})|L| - (2.83 \times 10^{-4})L^2 \quad (2)$$

where L represents the latitude in degrees. Note that no distinction between Northern and Southern latitudes is expected because of the symmetry of the orbits considered, so the results can also be expressed in terms of the absolute value of the latitude.

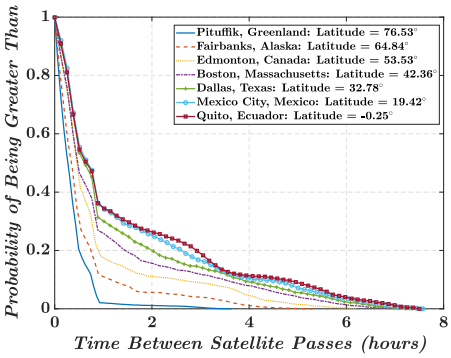

(a) Varied Latitudes

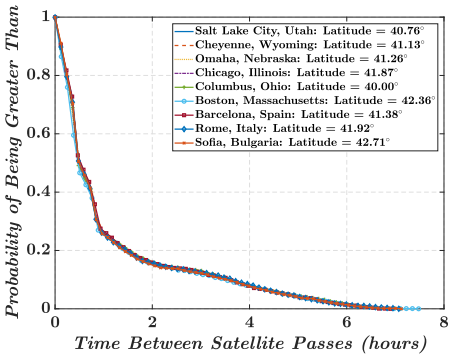

(b) Similar Latitudes

Fig. 2: Plot of the complementary cumulative distribution function of the time between successive of an EESS-passive satellite overpasses within the 100 km region surrounding cities of interest. (a) features seven cities with varying latitudes; (b) features nine cities with similar latitudes, but varying longitudes.

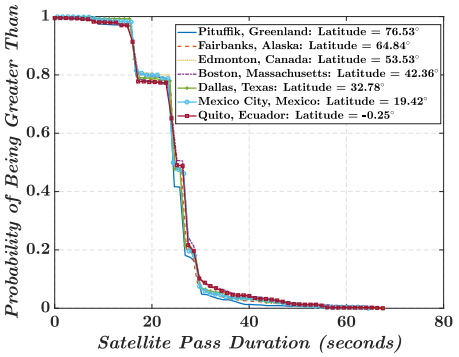

(a) Varied Latitudes

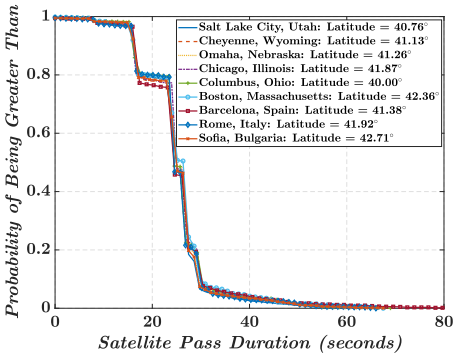

(b) Similar Latitudes

Fig. 3: Plot of the cumulative distribution function of the duration of an EESS-passive satellite overpass within the 100 km region of cities of interest. (a) features seven cities of varying latitudes; (b) features nine cities with of similar latitudes and varying longitudes.

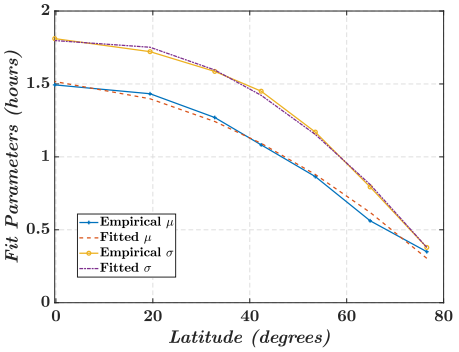

(a) Interarrival distributions

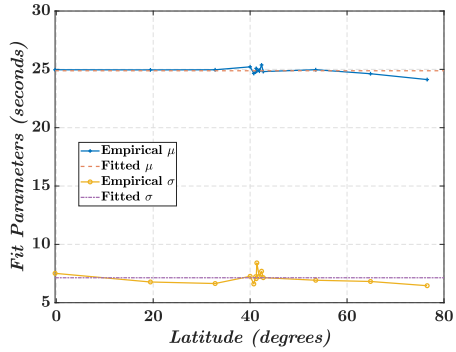

(b) Overpass distributions

Fig. 4: Plots the mean and standard deviation for the interarrival time distributions (hours) (a) and overpass duration distributions (seconds) (b) as a function of latitude as well as their respective fits.

B. Overpass Durations

In this section, we statistically characterize the overpass duration. Overpass durations are computed by first identifying the gaps between satellite arrivals as in the previous section and then computing the length of time during which measurements occurred between these gaps.

The plots of the resulting overpass duration CCDFs for multiple locations of varying latitudes and of similar latitude but varying longitudes are shown in Figs. 3(a) and (b), respectively. The resulting curves are similar for all locations, having a mean of $24.879s$ and a standard deviation of $7.139s$. The justification for a single value of the mean and standard deviation is shown in Fig. 4(b). The similarity of the curves for varying locations is expected given the 100 km radius applied for each site. The CCDFs show a steep drop-off at 15 seconds duration, followed by a plateau to approximately 18 seconds, a second plateau near 23 seconds, and a final decrease beginning around 30 seconds.

IV. Discussion

The distributions obtained in Figs. 2 and 3 do not appear highly similar to those of standard distributions. We conducted a Maximum Likelihood Estimation fit for a variety of distributions for both the interarrivals and overpass distributions. Because the interarrival CCDF has some attributes similar to an exponential distribution, we considered a number of distributions from the exponential family for comparison: the *Exponential*, *Gamma*, *Half-Normal*, and *Weibull* distributions as well as the *Log-Logistic* and *Log-Normal* distributions due to the heavy tail nature evident in the figures. For the overpass duration distributions, we considered a variety of heavy-tail distributions: the *Generalized Pareto*, *Logistic*, *Log-Logistic*, *Log-Normal*, and the *Weibull* distribution, as well as the *Exponential* distribution for comparison purposes (exponentially distributed service is a common default assumption in communications theory).

To evaluate the performance of each fit, we evaluate the R-Square error for each fit and location combination. The results are plotted in Fig. 5. For the interarrival time distributions, Fig. 5(a) shows that the log-normal MLE fit is the best of those tested. R-Square values for an exponential model remain approximately 0.9 or greater, so the exponential model may also be reasonable in some applications, particularly given the low service interruption rate and the analytical desirability of an exponential approximation in some methods. For the overpass duration distributions, Fig. 5(b) shows that the logistic fit performs best, but multiple random variable types achieve R-Square values near 0.9 and could be considered reasonable in particular applications. More generally, the empirical distributions are likely better described as a combination (i.e. convolution) of multiple distributions as a consequence of the multiple distinct types of radiometers included in the analysis. Analyses focused on the use of combined distributions will be reported in future work.

Overpass duration properties are particularly impacted by the varying scan types of distinct radiometers. Some systems (e.g. AMSR-2 and GMI) have a conically scanning antenna whose footprint scans through a semicircular swath as shown in Fig. 6(a) and (b). Observations in the area of interest can occur within a scan over azimuth and then in a subsequent scan separated by approximately 1.5 to 2 seconds. Other radiometers (AMSU-A) have a cross-track scan pattern producing the grid of observations shown in Fig. 6(c) that may be separated by approximately 6 to 8 seconds. Radiometers onboard altimeter missions (e.g. Sentinel 3A, Sentinel 6A) in contrast perform only a "single-spot" measurement at a fixed look angle (i.e. no scanning) as shown in Fig. 6(d). These differences in scan patterns result in different time delays between successive measurements and overpasses, with the "single-spot" radiometers having the longest time between repeat passes due to their narrow swath. The different scan types also result in varying amounts of time over an area of interest, consistent with the "multi-scale" attributes of the duration distribution observed in Fig. 3(b).

V. Application to Economic Modeling

The variety of overpass properties reinforces the desire for a stochastic view of service interruptions, as economic models are interested in overall utilization. Indeed, we find regardless of latitude, EESS-passive radiometers utilize spectrum for a relatively small fraction of time. Fig. 8 plots the mean fraction of time that is not used in radiometer observation. From south of the Arctic Circle (latitude 66.85) to the Equator, service is uninterrupted for more than 99% of the time, peaking at 99.56% at the Equator. These percentages assume the spectrum of interest is rendered unavailable when the radiometer is present, i.e. the most restrictive buffer possible and thus represent the *worst* case from a commercial user perspective. It is this low level of utilization even in the face of such restrictions that promotes potential co-existence on bands utilized by the radiometers. From an economic perspective, (wholesale) spectrum pricing models based on the availability of the remaining spectrum can be tuned based on location without specific knowledge of the forecast arrivals of incoming radiometers. To demonstrate this, we revisit the Open Access economic model of [27] as an example. In this model, customers are willing to purchase spectrum access if they achieve higher utility by joining the system rather than balking (i.e., not joining the system). The objective of the service provider is to maximize the fee which can be charged, taking also into consideration the sensitivity of the customer to delay and preemptions caused by EESS-passive use.

Under this framework, we consider scenarios featuring high delay sensitivity (defined here as jobs which must complete within 10 seconds of entering the system) and low delay sensitivity (jobs which must complete within 100 seconds of entering the system). In both cases, we consider scenarios where preemption incurs costs of 1, 10, and 100 times the reward of service. In Figs. 7(a) and (b) we plot the per-second wholesale Open Access profits in each scenario. We plot both the empirical results from each location in Table II, and the estimation from our studies in Sections III. The customer

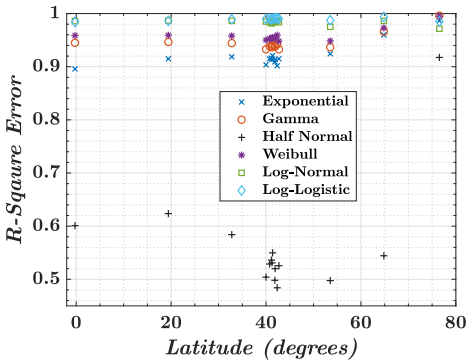

(a) Interarrivals

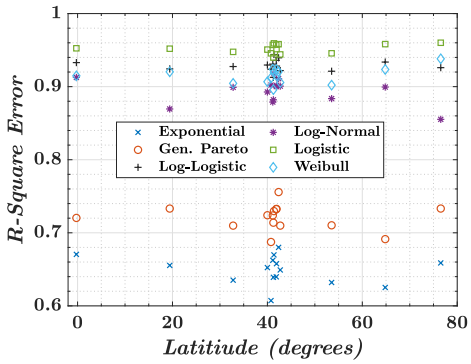

(b) Overpass Durations

Fig. 5: Plots of the R-Square error for various Maximum Likelihood Estimation fitted distributions for the interarrival time (a) and overpass duration (b) at each location from Table II. For the interarrival times, while log-normal is the best fit, any of the distributions other than the Half-Normal can be considered reasonable approximations. Similarly, for overpass lengths the logistic distribution provides the best fit but there exist other alternatives that also provide reasonable approximations (principally the related Log-Normal and Log-Logistic distributions).

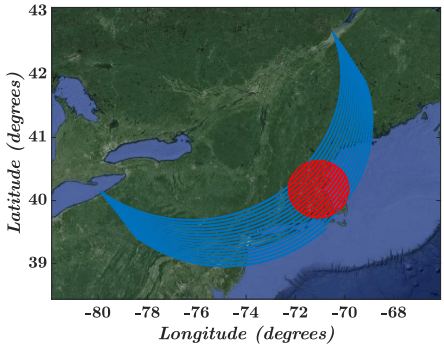

(a) GMI scan pattern

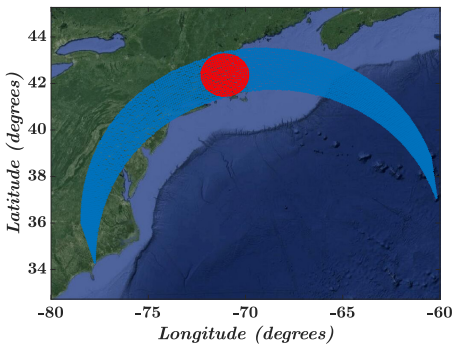

(b) AMSR-2 scan pattern

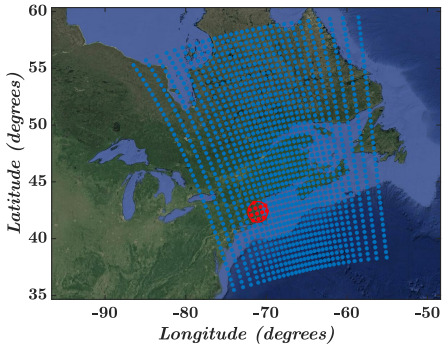

(c) AMSU scan pattern

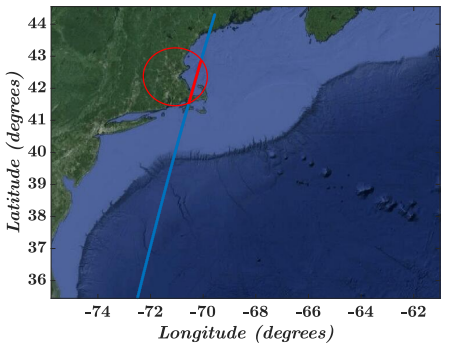

(d) Altimeter scan pattern

Fig. 6: Plots of the scan pattern for different radiometers (a) conical scan from GMI (b) conical scan from AMSR-2 (c) cross-track scan from AMSU (d) radiometer aboard altimeter satellite. The large red circle corresponds to the 100 km selected area of interest region around Boston, Massachusetts. The smaller red points correspond to measurements co-located within the red circle area. The blue points are measurements located outside the selected area of interest.

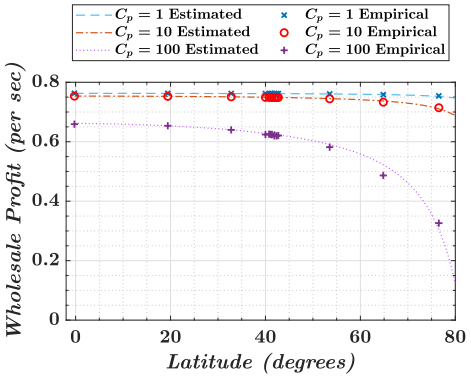

(a) Low Delay Sensitivity

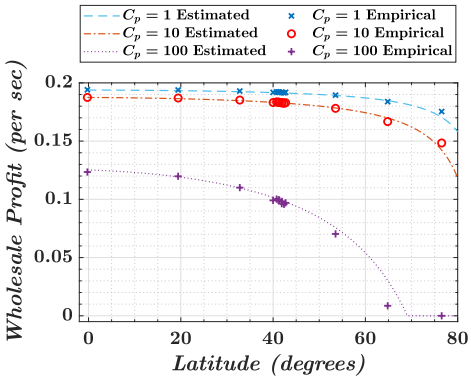

(b) High Delay Sensitivity

Fig. 7: Plot of the profit maximizing fee vs latitude under scenarios derived from the Open Access model in [27], for each location in Table II and the estimated mean interarrival times and overpass periods in Subsections III-A and III-B. We consider scenarios corresponding to (a) low delay sensitivity (jobs must complete within $100s$ of entering the system) and (b) high delay sensitivity (jobs must completely within $10s$) and varying levels of sensitivity to preemption (1, 10, and 100 times the reward per-preemption) as examples.

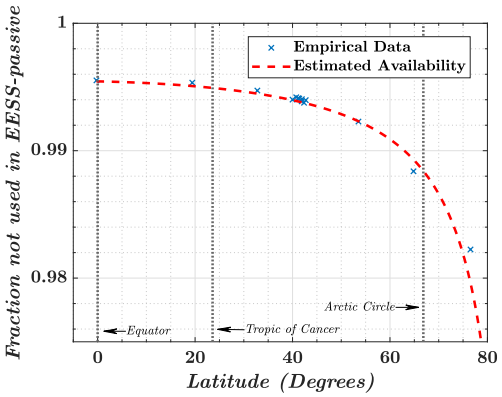

Fig. 8: Plot of the average fraction of time not used by radiometers at each location (symbols) and associated curve fit.

traffic statistics used here are from [28]: Poisson distributed arrivals with a mean interarrival time of $7.25s$, and a service distribution with mean service time of $6.47s$ and a standard deviation of $1.78s$.

We see in Fig. 7(a) that in the low delay sensitivity case *there is a definite correlation between latitude and the maximum profit that a provider can achieve*. This is most pronounced in the high preemption sensitivity case. This is expected; as the only preemptions possible under the model are from the radiometers. Under a low-delay high-preemption sensitivity scenario, the maximum profit per time unit achievable at Quito, near the equator, is 2.5 times greater than that at Pituffik, inside the Arctic Circle. This holds even though the amount of available spectrum to non EESS-passive users at Quito is only 1.01 times that at Pituffik (i.e., 1 percent greater).

In Fig. 7(b), we consider the high delay sensitivity case. While the corresponding profits are lower than in the low delay sensitivity case, the same phenomenon where the correlation between latitude and profit becomes most pronounced as preemption sensitivity increases is apparent, to the point where a situation occurs at polar latitudes where no customers are willing to join the system, resulting in 0 profits. These results demonstrate the extent of the impact that changes in EESS-passive access can have on commercial user incentives. Depending on the nature of the scenario, particularly customers' sensitivity to quality of service factors, the changes in EESS-passive access at higher latitudes can be significant compared to those at the equator. This is an important factor, which to the best of our knowledge, previous economic models of spectrum sharing did not consider. As a result, knowledge of the estimated data enables planning within an economic model to be tuned by location of the service area, rather than attempting to apply a universal assumption on the EESS-passive utilization or requiring trace data for every given location of interest. In turn, this simplifies planning while enabling a baseline availability to be calculated at a granular level to provide a more flexible service to varying locations.

VI. Conclusion

The interarrival times and durations of EESS-passive satellite overpasses are of interest to those investigating the possibility of future spectrum sharing paradigms. The interarrival time CCDFs investigated had a clear dependence on latitude, with mean and standard deviations well matched by a quadratic least squares fit versus latitude. In contrast, the CCDFs of overpass durations showed no significant dependence on location and showed a mean of $24.879s$ and standard deviation $7.139s$. While the distributions obtained appear more complex than standard simple forms, a goodness-of-fit test

showed that they could be approximated by simple forms in some applications. For instance, economic interactions which are tied to spectrum availability, especially those where users are highly sensitive to service interruptions, will result in a strong correlation between the target service location, the estimated EESS-passive utilization rate via estimated arrival rate, and provider profits as demonstrated by the example model employed in Section V.

Follow-on work with these statistical characterizations will likely involve attempting to separate the multiple distributions from the data, as well as further economic and policy applications to refine assumptions on utilization rates and availability to enable systems planning for co-existence regimes between commercial users and EESS-passive on scales larger than individual cites. In addition to further fine-tuning of underlying commercial user behaviors, this requires a degree of cooperation across a wide area, which lends itself to a statistical view of the EESS-passive as opposed to attempting to analyze trace data for each individual location. Finally, applications of the statistical analysis include leveraging refined fits to simulated data in support of game-theoretic analysis to ensure accuracy in results where utilizing a defined statistical distribution is necessary and exact trace data utilization is not practicable.

ACKNOWLEDGMENT

This research was supported in part by the NSF under grants AST-2229103 and AST-2229104.

The views expressed are those of the authors and do not reflect the official guidance or position of the United States Government, the Department of Defense, the United States Air Force, or the United States Space Force.

REFERENCES

[1] "Handbook of frequency allocations and spectrum protection for scientific uses," 500 Fifth Street, NW Washington, DC 20001, pp. 52–85, 2015. [Online]. Available: https://doi.org/10.17226/21774

[2] "Spectrum management for science in the 21st century," 500 Fifth Street, NW Washington, DC 20001, pp. 18–87, 2010. [Online]. Available: https://doi.org/10.17226/12800

[3] E. R. Westwater, Y. Han, M. D. Shupe, and S. Y. Matrosov, "Analysis of integrated cloud liquid and precipitable water vapor retrievals from microwave radiometers during the surface heat budget of the arctic ocean project," *Journal of Geophysical Research: Atmospheres*, vol. 106, no. D23, pp. 32 019–32 030, 2001. [Online]. Available: https://agupubs.onlinelibrary.wiley.com/doi/abs/10.1029/2000JD000055

[4] J. Houts and E. Kim, "The spectrum outlook for earth remote sensing post WRC-19," in *IGARSS 2020 - 2020 IEEE International Geoscience and Remote Sensing Symposium*, 2020, pp. 3778–3780.

[5] T. Meissner and F. J. Wentz, "The emissivity of the ocean surface between 6 and 90 GHz over a large range of wind speeds and earth incidence angles," *IEEE Transactions on Geoscience and Remote Sensing*, vol. 50, no. 8, pp. 3004–3026, 2012.

[6] Y. Soldo, F. Jorge, K. Andersen, B. Espinosa, M. Dreis, and J. Roselló, "Decisions of the world radiocommunication conference 2023 and their impact on earth observations," in *IGARSS 2024 - 2024 IEEE International Geoscience and Remote Sensing Symposium*, 2024, pp. 756–758.

[7] NASA, "AIRS/Aqua L1B AMSU (A1/A2) geolocated and calibrated brightness temperatures V005," Accessed: November 20, 2023. [Online]. Available: https://disc.gsfc.nasa.gov/datasets/AIRABRAD_005/summary

[8] JAXA, "GCOM-W AMSR-2 level 1 brightness temperature data," Accessed: November 20, 2023. [Online]. Available: https://gportal.jaxa.jp/gpr/search?tab=1

[9] NASA, "GPM GMI brightness temperatures L1B 1.5 hours 13 km V07," Accessed: November 20, 2023. [Online]. Available: https://disc.gsfc.nasa.gov/datasets/GPM_1BGMI_07/summary

[10] EUMETSAT, "AMSU-A level 1B data - metop," Accessed: November 20, 2023. [Online]. Available: https://data.eumetsat.int/product/EO:EUM:DAT:METOP:AMSUL1

[11] NOAA, "MSU/AMSU-A brightness temperature - NOAA climate data record (CDR)," Accessed: November 20, 2023. [Online]. Available: https://www.ncei.noaa.gov/has/HAS.FileAppRouter?datasetname=NSTAR_FCDR&subqueryby=STATION&applname=&outdest=FILE

[12] ——, "Index of /data/amsu-a-brightness-temperature/access," Accessed: November 20, 2023. [Online]. Available: https://www.ncei.noaa.gov/data/amsu-a-brightness-temperature/access

[13] ——, "NOAA JPSS advanced technology microwave sounder (ATMS) temperature data record (TDR) from IDPS," Accessed: November 20, 2023. [Online]. Available: https://www.ncei.noaa.gov/access/metadata/landing-page/bin/iso?id=gov.noaa.ncdc:C01426

[14] ESA, "Sentinel-3 SRAL level 2 data," Accessed: November 20, 2023. [Online]. Available: https://documentation.dataspace.copernicus.eu/Data/Sentinel3.html#sentinel-3-sral-level-2

[15] EUMETSAT, "Climate-quality advanced microwave radiometer level 2 products in NRT - sentinel-6," Accessed November 20, 2023. [Online]. Available: https://navigator.eumetsat.int/product/EO:EUM:DAT:0146

[16] NASA, "SWOT level 2 radiometer brightness temperatures and troposphere data product," Accessed June 20, 2024. [Online]. Available: https://podaac.jpl.nasa.gov/dataset/SWOT_L2_RAD_GDR_2

[17] B. Agarwal, M. A. Togou, M. Marco, and G.-M. Muntean, "A comprehensive survey on radio resource management in 5G hetnets: Current solutions, future trends and open issues," *IEEE Communications Surveys & Tutorials*, vol. 24, no. 4, pp. 2495–2534, 2022.

[18] I. F. Akyildiz, A. Kak, and S. Nie, "6G and beyond: The future of wireless communications systems," *IEEE Access*, vol. 8, pp. 133 995–134 030, 2020.

[19] M. Andrews, H. Li, J. T. Johnson, K. C. Jezek, A. Bringer, C. Yardim, C.-C. Chen, D. Belgiovane, V. Leuski, M. Durand, Y. Duan, G. Macelloni, M. Brogioni, S. Tan, and L. Tsang, "The ultra-wideband software defined microwave radiometer (UWBRAD) for ice sheet subsurface temperature sensing: Calibration and campaign results," in *2017 IEEE International Geoscience and Remote Sensing Symposium (IGARSS)*, 2017, pp. 237–240.

[20] F. D. Lind, S. Thé, D. Sheen, A. P. Stefania, G. Rajagopalan, and M. Poirier, "Initial observations of starlink satellites using the westford radio telescope," in *2024 IEEE International Symposium on Dynamic Spectrum Access Networks (DySPAN)*, 2024, pp. 1–6.

[21] S. Munira, D. Saha, G. Hellbourg, and A. Dutta, "Dynamic protection zone for radio astronomy," in *2024 IEEE International Symposium on Dynamic Spectrum Access Networks (DySPAN)*, 2024, pp. 556–560.

[22] E. Eichen, "Real-time geographical spectrum sharing by 5G networks and earth exploration satellite services," in *2019 IEEE International Symposium on Dynamic Spectrum Access Networks (DySPAN)*, 2019, pp. 1–2.

[23] ——, "Performance of real-time geospatial spectrum sharing (RGSS) between 5G communication networks and earth exploration satellite services," in *2021 IEEE International Symposium on Dynamic Spectrum Access Networks (DySPAN)*, 2021, pp. 73–79.

[24] M. J. Marcus, "Progress in opening access to spectrum above 100 GHz," *IEEE Wireless Communications*, vol. 26, no. 2, pp. 2–3, 2019.

[25] M. Polese, X. Cantos-Roman, A. Singh, M. J. Marcus, T. J. Maccarone, T. Melodia, and J. M. Jornet, "Coexistence and spectrum sharing above 100 GHz," *Proceedings of the IEEE*, vol. 111, no. 8, pp. 928–954, 2023.

[26] J. Chamberlain, D. Starobinski, and J. T. Johnson, "Facilitating spectrum sharing with passive satellite incumbents," *IEEE Journal on Selected Areas in Communications*, pp. 1–1, 2024.

[27] J. Chamberlain, J. Johnson, and D. Starobinski, "Spectrum sharing between earth exploration satellite and commercial services: An economic feasibility analysis," in *2024 IEEE International Symposium on Dynamic Spectrum Access Networks (DySpan)*, 2024, pp. 197–206.

[28] M. Lopez-Benitez and F. Casadevall, "Time-dimension models of spectrum usage for the analysis, design, and simulation of cognitive radio networks," *IEEE transactions on vehicular technology*, vol. 62, no. 5, pp. 2091–2104, 2013.